Reactions induced by ^{13}C on ^{12}C, ^{16}O, ^{28}Si, and ^{32}S†

Gary D. Westfall* and S. A. A. Zaidi
The University of Texas at Austin, Austin, Texas 78712
(Received 2 October 1975)

Angular distributions for the reactions $^{12}C(^{13}C,^{13}C)^{12}C$, $^{12}C(^{13}C,^{9}Be)^{16}O$, $^{16}O(^{13}C,^{13}C)^{16}O$, $^{16}O(^{13}C,^{12}C)^{17}O^*$ (0.871 MeV), $^{28}Si(^{13}C,^{13}C)^{28}Si$, $^{28}Si(^{13}C,^{12}C)^{29}Si$; $^{28}Si(^{13}C,^{12}C)^{29}Si^*$ (1.27 MeV), $^{28}Si(^{13}C,^{14}N)^{27}Al$, $^{32}S(^{13}C,^{13}C)^{32}S$, $^{32}S(^{13}C,^{12}C)^{33}S$, $^{32}S(^{13}C,^{12}C)^{33}S^*$ (0.841 MeV), and $^{32}S(^{13}C,^{14}N)^{31}P$ have been measured in fine steps between $\theta_{lab} = 4°$ and $\theta_{lab} = 40°$ at the bombarding energy of 36 MeV. Elastic scattering data are fitted by optical-model calculations and the parameters of the potential are determined. The neutron-transfer and proton-pickup reaction cross sections are compared with the predictions of the exact finite-range distorted-wave Born-approximation. The calculated angular distributions reproduce the gross features of the data but not the details. The quantitative agreement of the determined spectroscopic factors with the spectroscopic factors found from light-ion reactions varies from excellent to poor. The α-transfer reaction $^{12}C(^{13}C,^{9}Be)^{16}O$ has been analyzed using cluster-model form factors. The agreement between theory and experiment is poor. The measured angular distribution is, however, well described by $|P_{10}(\cos\theta)|^2$.

[NUCLEAR REACTIONS Elastic scattering, neutron stripping, and proton pickup induced by 36 MeV ^{13}C on ^{32}S, ^{28}Si, ^{16}O, and ^{12}C, and $^{12}C(^{13}C,^{9}Be)^{16}O$ measured at $\theta_{lab} = 4°–40°$, $\Delta\theta_{lab} = 1°$. Optical-model parameters, exact finite-range DWBA, spectroscopic factors.]

I. INTRODUCTION

In recent years extensive studies of heavy-ion induced reactions have led to a quantitative understanding of the reaction mechanisms involved in several types of such reactions. This is particularly true of the one-nucleon transfer reactions that have been the subject of careful and systematic investigations at several laboratories.[1-5] The semiclassical aspects of the heavy-ion collisions have formed the basis of several models,[6-9] and gross features of the observed angular distributions can, in many cases, be understood in terms of these models. For a quantitative understanding of the reactions, and in particular for the extraction of spectroscopic factors it is necessary to use the distorted-wave theory of reactions. For applications to heavy-ion reactions, the commonly used zero-range approximation has to be abandoned. Recently, computer codes[10,11] for performing exact finite-range distorted-wave Born-approximation (EFR DWBA) calculations have become available. It is of considerable interest to compare neutron-transfer and proton-pickup reactions induced by heavy projectiles with the corresponding (d,p) and $(d,^3He)$ reactions. The projectile ^{13}C appears to be well suited for one-neutron-transfer reactions because of its extra neutron.

In the past, ^{13}C induced reactions have received limited attention. Gobbi[12] and Chua *et al.*[13] analyzed the elastic and inelastic scattering of the $^{12}C + ^{13}C$ system with a view to discuss the contributions of elastic and inelastic transfer. Debevec, Körner, and Schiffer[14] measured excitation functions and angular distributions of the reaction $^{13}C(^{16}O,^{17}O)^{12}C$ to demonstrate that resonances observed in the $^{16}O + ^{12}C$ system persisted in $^{16}O + ^{13}C$ system. Seiler *et al.*[15] measured excitation functions of the total cross sections for one-neutron-transfer reactions by detecting the deexcitation γ rays. They also reported measurements of lifetimes of final states. To our knowledge, no ^{13}C induced reactions on ^{28}Si or ^{32}S have been reported in the literature.

In the present study, the cross sections for elastic scattering of ^{13}C from ^{12}C, ^{16}O, ^{28}Si, and ^{32}S were measured in fine steps in the angular range between $\theta_{lab} = 4°$ and $\theta_{lab} = 40°$. This was done for the purpose of determining optical-model parameters for these channels. Angular distributions for the transfer reactions $^{32}S(^{13}C,^{12}C)^{33}S$, $^{32}S(^{13}C,^{12}C)^{33}S^*$ (0.841 MeV), $^{32}S(^{13}C,^{14}N)^{31}P$, $^{28}Si(^{13}C,^{12}C)^{28}Si$, $^{28}Si(^{13}C,^{12}C)^{29}Si^*$ (1.27 MeV), $^{28}Si(^{13}C,^{14}N)^{27}Al$, $^{16}O(^{13}C,^{12}C)^{17}O^*$ (0.871 MeV), and $^{12}C(^{13}C,^{9}Be)^{16}O$ were measured in fine steps over the same angular range and the results were compared with EFR DWBA calculations. The cross section for the α-transfer reaction is compared with EFR DWBA calculations and with $|P_l(\cos\theta)|^2$, where l is the orbital angular momentum for the classical grazing trajectory of ^{13}C incident on ^{12}C.

II. EXPERIMENTAL METHOD

The experiments reported here were performed with the 36 MeV ^{13}C beam from the University of Texas EN tandem Van de Graaff accelerator. ^{13}C ions were produced in a cesium sputter ion source.[16] The intensity of the ^{13}C beam used in this experiment varied between 50 and 300 nA.

The scattering chamber used was 1 m in diameter. Two different detector configurations were used. The first configuration consisted of four silicon surface-barrier detectors, each 200 μm thick, mounted 10° apart. The second configuration consisted of a monitor detector and a particle telescope. The telescope was made up of two surface-barrier detectors, a 10.7 μm ΔE detector and a 200 μm E detector. Particle identification using the telescope was based on the linear relationship between dE/dx and E for the scattered particles in our energy range. Values for dE/dx were taken from the tables of Northcliffe and Schilling.[17] Since the values of dE/dx were not tabulated for Si, the values of dE/dx for ions passing through Al were taken. Figure 1 shows the graph of $-dE/dx$ versus E for ^{14}N ions passing through Al. In this energy region, one can express the linear relationship between E and dE/dx as

$$-\frac{dE}{dx} = bE + c\,, \tag{1}$$

where b is the slope of the linear region and c is the y intercept of the extrapolated straight line. Similar relationships are valid for several projectiles of neighboring values of charge and mass. One notices that c depends strongly on the particle type, whereas b is almost independent of it. This expression can be integrated over the thickness T of the ΔE detector to give

$$E + A\Delta E = B\,, \tag{2}$$

where

$$A = [1 - \exp(bT)]^{-1}\,, \tag{3}$$

and

$$B = -c/b\,. \tag{4}$$

Here ΔE is the energy lost by the particle in passing through the ΔE detector and E is the energy of the particle striking the E detector. The factor A is nearly independent of the charge and mass of the particle. It was calculated to be approximately 6. The value for B is dependent on the charge and mass of the particle and the predicted values of B can be used to identify the various particles.

The pulses from the two detectors were digitally summed, in addition the function $E + A\Delta E$ was formed to identify the detected particles. Gates were set on the peaks in the identification spectrum corresponding to the different particles and the corresponding energy spectra were selected. The actual value of A used was found empirically by displaying the $E + \Delta E$ spectrum versus the $E + A\Delta E$ spectrum and choosing the value of A which best linearized the display. This value was found to be 12. We attribute this discrepancy to the numerical values of dE/dx used. The above reasoning, however, seems to justify the use of Eq. (2) as an empirical relationship. The telescope was able to discriminate between particles differing in one unit of charge but could not resolve particles differing in one unit of mass. A typical particle-identification spectrum is shown in Fig. 2.

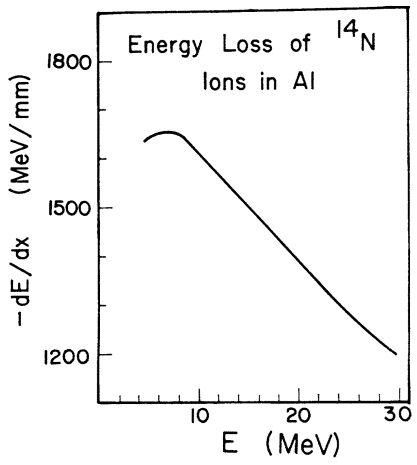

FIG. 1. Rate of energy loss for nitrogen ions in aluminum. The curve is based on tables by Northcliffe and Schilling (Ref. 17) and shows that for energy values between 10 and 25 MeV there is a linear relationship between dE/dx and E.

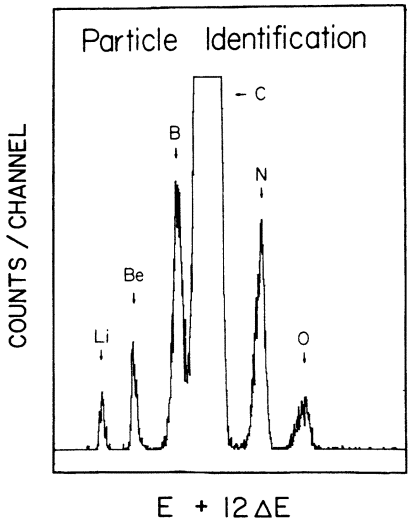

FIG. 2. Particle identification spectrum showing that particles differing in one unit of charge are clearly separated.

Four different natural targets were used. For a ^{12}C target, self-supporting carbon foils were used varying in thickness from 10 to 100 $\mu g/cm^2$. A self-supporting SiO target was used for ^{28}Si and ^{16}O which was approximately 30 $\mu g/cm^2$ thick. Li_2S evaporated onto a carbon backing produced a ^{32}S target of approximately 6 $\mu g/cm^2$ thickness. No significant deterioration was observed during the experiment in any of the above targets.

The beam spot was limited to 1 mm width and 12 mm height and the angular acceptance of the detectors was limited to approximately $\frac{1}{8}^\circ$. The energy resolution varied between 180 and 280 keV full width at half maximum (FWHM).

The absolute cross sections were found by assuming the observed elastic scattering to be Rutherford scattering at the smallest scattering angle for which data were taken. The reaction cross sections were found from the ratio of the yields in the reaction peaks to the yield in the elastic peaks.

The particle telescope did not allow a discrimination between ^{12}C and ^{13}C. In the angular range of interest, however, the detected particles arising from an elastic collision between a ^{12}C target and ^{13}C projectile consist almost exclusively of ^{13}C. This fact may be seen as follows: The observed cross section $\bar{d}\bar{\sigma}/d\Omega$ may be written as:

$$\frac{\bar{d}\bar{\sigma}}{d\Omega}(\theta)=\frac{d\sigma}{d\Omega}(\theta)+\frac{d\sigma}{d\Omega}(\text{recoil angle}=\theta)\,, \qquad (5)$$

where $d\sigma/d\Omega$ (recoil angle $=\theta$) is the cross section for the recoiling nucleus ^{12}C to be detected at the angle θ and $d\sigma/d\Omega(\theta)$ is the cross section for ^{13}C to be detected at an angle θ. The ratio

$$\frac{d\sigma}{d\Omega}(\text{recoil angle}=\theta)\Big/\frac{d\sigma}{d\Omega}(\theta)$$

can be rewritten by expressing these cross sections in terms of the corresponding cross sections for the scattering of ^{13}C on ^{12}C in the center-of-mass frame and the Jacobians of the transformation evaluated at the appropriate angles. The ratio of these two center-of-mass cross sections is finally estimated on the basis of known[12] cross sections for this reaction at other energies. In this manner we arrive at an upper limit of 2×10^{-4} at 4° and 3% at 40° for this ratio. Accordingly we ignore the second term in (5).

III. ANALYSIS OF ELASTIC SCATTERING DATA

The measured elastic scattering cross sections were compared with elastic scattering cross sections calculated for an optical-model potential of Woods-Saxon shape. The computer code OMFESD[18] (Optical Model Fit to Elastic Scattering Data) was used to perform these calculations and to search for the parameters of the optical potential that produced the best fit to the data. The six parameters determining the Woods-Saxon potential that were searched upon were as follows: well depths, radius parameters, and diffusenesses of the real and imaginary parts of the optical-model potential. The imaginary part of the optical-model potential was taken to be purely of volume type. Two parameters were searched at a time in an effort to minimize the χ^2 and the procedure was repeated about 15 times until it was felt that no further improvement could be achieved. We found several different sets of parameters that provided very good fits to the data. The parameters for the best fit in each case are given in Table I. The ambiguity in optical-model parameters for heavy ions arising from the circumstance that only the "tail region" of the potential determines the scattering is well known.[19] Reference 20 gives a particularly clear formulation of the transformation relating equivalent sets of optical-model parameters.

Figure 3 shows the cross sections in the center-of-mass frame for the elastic scattering of ^{13}C from ^{12}C, ^{16}O, ^{28}Si, and ^{32}S at 36 MeV bombarding energy. Also shown in the same figure are the optical-model calculation for the parameters given in Table I. In the case of ^{32}S, apart from a small discrepancy around $\theta_{c.m.}=30^\circ$, the calculated cross sections agree perfectly with the measured cross sections. The ^{28}Si elastic scattering data display small oscillations superimposed on a gradual fall-off. Also in this case, the agreement between measured and calculated cross sections is very good. Elastic scattering data for ^{16}O and ^{12}C display well

TABLE I. Optical-model parameters for best fit.

Reaction	V (MeV)	r_0 (fm)	a_0 (fm)	W (MeV)	r_I (fm)	a_I (fm)
$^{32}S(^{13}C,^{13}C)^{32}S$	100.166	1.235	0.507	8.489	1.234	0.889
$^{28}Si(^{13}C,^{13}C)^{28}Si$	112.12	1.177	0.524	10.087	1.324	0.304
$^{28}Si(^{12}C,^{12}C)^{28}Si$ [a]	90.624	1.173	0.530	10.036	1.295	0.317
$^{16}O(^{13}C,^{13}C)^{16}O$	100.323	1.140	0.560	12.960	1.284	0.442
$^{12}C(^{13}C,^{13}C)^{12}C$	86.602	1.084	0.586	9.563	1.263	0.329

[a] $E_{lab}=40.16$ MeV.

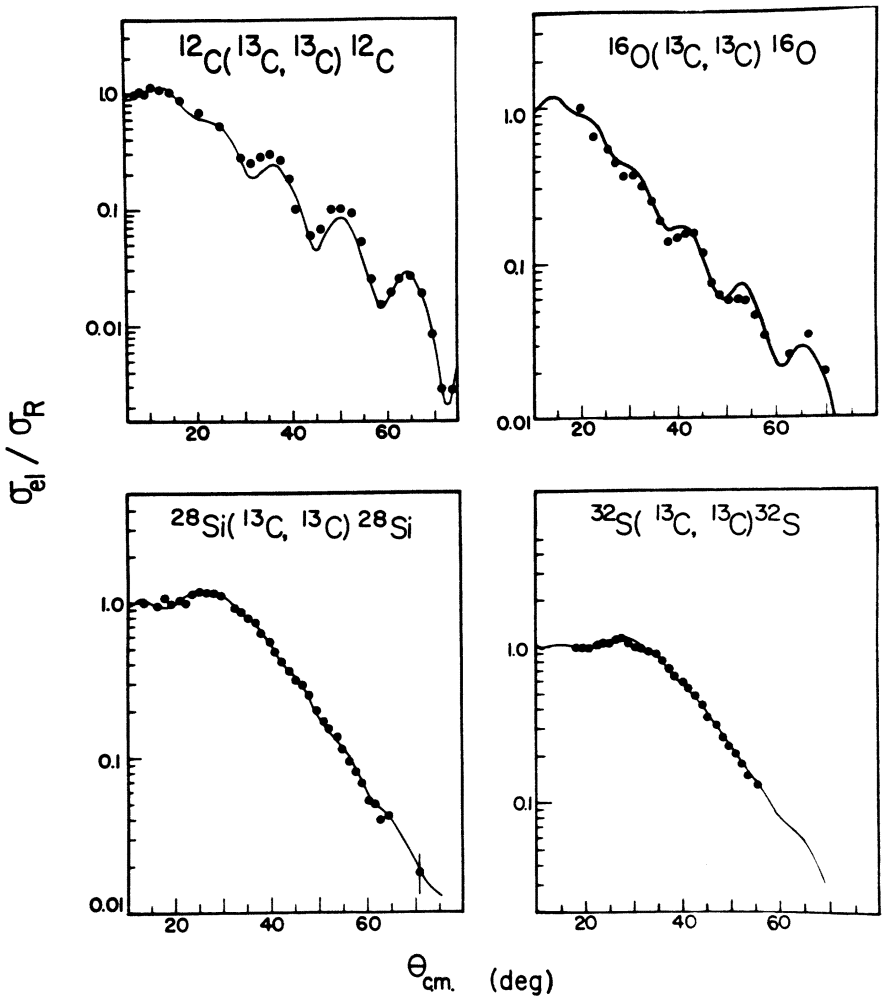

FIG. 3. Cross sections for the elastic scattering of 36 MeV ^{13}C from ^{12}C, ^{16}O, ^{28}Si, and ^{32}S. Optical-model calculations for the best-fit parameters given in Table I are shown as solid lines. Scattering cross section at the smallest angle in each case was assumed to be given by Rutherford's formula.

pronounced oscillations. Also in these two cases, the calculations provide a good fit to the data. It is apparent, however, that there are definite though small discrepancies between the data and the calculations. These discrepancies persisted in spite of considerable effort to search for more suitable parameters by varying them two at a time.

The absolute cross sections were arrived at by assuming that the cross section measured at the smallest scattering angle was in each case equal to the Rutherford scattering cross section at that angle. This assumption is justified *a posteriori* for the elastic scattering from ^{12}C, ^{28}Si, and ^{32}S as evidenced by the flattening out of the ratio σ_{el}/σ_R. In the case of ^{16}O our data do not justify this assumption. However, we estimate that the uncertainty introduced in the absolute normalization is less than 15%.

In addition to the elastic scattering of ^{13}C from ^{28}Si at 36 MeV, the elastic scattering of ^{12}C from ^{28}Si at 40.16 MeV was also measured. This measurement was carried out to describe the elastic scattering in the exit channel of the reaction $^{28}Si(^{13}C, ^{12}C)^{29}Si$. An optical-model fit was obtained to the data and the parameters found are listed in Table I. The cross sections in the center-of-mass frame are shown in Fig. 4 along with the optical-model fit.

IV. REACTION DATA AND ANALYSIS

Reaction data obtained in this experiment were compared with EFR DWBA calculations using the computer code SATURN-MARS by Tamura and Low.[10] The optical-model parameters needed to generate the distorted waves were obtained as described in the previous section. The optical-model param-

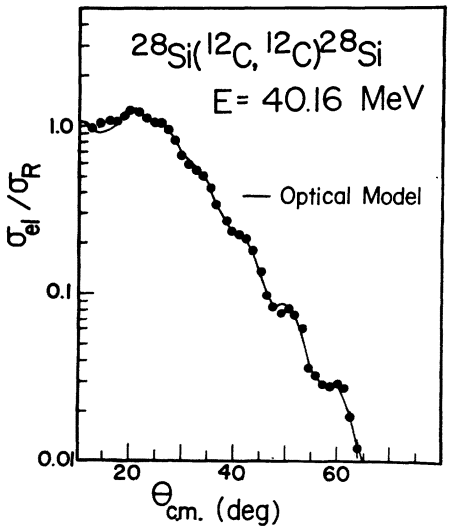

FIG. 4. Cross sections for the elastic scattering of 40.16 MeV ^{12}C from ^{28}Si. Optical-model calculation for the best-fit parameters given in Table I is shown as solid line. Scattering cross section at the smallest angle was assumed to be given by Rutherford's formula.

eters for the exit channel were obtained from those of the entrance channel by scaling the radii with $(A_1^{1/3}+A_2^{1/3})$. Some additional calculations were performed for the one-neutron-transfer reaction on ^{28}Si in which the optical-model parameters of the exit channel were varied. The post form of the DWBA transition matrix element was used in calculations describing the pickup reactions. Sixty partial waves were used in each of the two channels and it was ascertained that the contribution from the last 10 partial waves was negligible. Bound state wave functions were calculated using a Woods-Saxon potential with the radius parameter r_0 equal to 1.2 fm, the diffuseness a equal to 0.65 fm, and the depth V equal to the value which reproduced the binding energy of the transferred particle.

The product of the two spectroscopic factors involved in each reaction was determined by requiring a visual fit of the calculation to the observed data. In the neutron-transfer reactions discussed below, the spectroscopic factors of the final states of the nuclei were obtained by assuming the neutron spectroscopic factor of the ground state of ^{13}C. Several experimental investigations have been concerned with this spectroscopic factor.[21] The values obtained lie within the range 0.6–1.2. We assumed a value of 0.61 predicted by Cohen and Kurath[22] for the analysis presented here. The proton spectroscopic factor for the ground state of ^{14}N was needed for extracting the proton spectroscopic factors of the target nuclei in the pickup reactions. It was also taken from the calculations by Cohen and Kurath to be 0.69 since consistent experimental values were not available. The derived spectroscopic factors are compared with those found from (d,p) and $(d,{}^3He)$ reactions for the neutron-transfer and proton-pickup reactions, respectively. Table II lists these spectroscopic factors as well as the Q value, the excitation and spin and parity of the final state of the residual nucleus, the allowed l transfer, and the derived bound state well depth for each reaction.

All reaction data are shown in the center-of-mass frame of reference.

TABLE II. Spectroscopic factors for the neutron-transfer and proton-pickup reactions induced by ^{13}C.

Reaction	Q value (MeV)	E_{exc} (MeV)	J^π	Allowed l transfer	Bound state well depth (MeV)	C^2S This work		C^2S From light-ion studies
						Same [e]	Different [e]	
$^{32}S(^{13}C,{}^{12}C)^{33}S$	3.69	0.0	$\frac{3}{2}^+$	1,2	52.4	1.64		0.93 [a]
$^{32}S(^{13}C,{}^{12}C)^{33}S^*$	3.69	0.841	$\frac{1}{2}^+$	1	48.2	0.48		0.32 [a]
$^{32}S(^{13}C,{}^{14}N)^{31}P$	−1.31	0.0	$\frac{1}{2}^+$	1	61.5	1.66		1.1 [b]
$^{28}Si(^{13}C,{}^{12}C)^{29}Si$	3.53	0.0	$\frac{1}{2}^+$	1	52.7	0.51	0.47	0.53 [a]
$^{28}Si(^{13}C,{}^{12}C)^{29}Si^*$	3.53	1.27	$\frac{3}{2}^+$	1,2	54.1	0.96	0.89	0.74 [a]
$^{28}Si(^{13}C,{}^{14}N)^{27}Al$	−4.03	0.0	$\frac{5}{2}^+$	2,3	63.4	2.9		3.3 [c]
$^{16}O(^{13}C,{}^{12}C)^{17}O^*$	−0.804	0.871	$\frac{1}{2}^+$	1	56.9	0.49		0.78 −0.91 [d]

[a] From Ref. 25.
[b] From Ref. 29.
[c] From Ref. 30.
[d] From Ref. 26. An earlier work, Ref. 27, gave 0.62 and Ref. 28 leads to a range of values between 0.5 and 1.0 depending upon the deuteron energy.
[e] See Sec. IV B and Fig. 7 for explanation.

A. Reactions induced on ^{32}S

Experimental cross sections for the reaction $^{32}S(^{13}C, ^{12}C)^{33}S$ leading to the ground state and first excited state of ^{33}S are shown in Fig. 5 along with the EFR DWBA calculations. In the case of the ground state, poor agreement between the calculated and measured cross sections and large statistical errors in the data make the determination of the spectroscopic factor uncertain. The first excited state is not expected to be a very pure single-particle state since the $2S_{1/2}$ single-particle orbit is expected to be filled in ^{33}S on the basis of simple shell-model considerations. Experimental cross sections for the proton-pickup reaction $^{32}S(^{13}C, ^{14}N)^{31}P$ are shown in Fig. 6 along with an EFR DWBA calculation. The calculated cross sections for the neutron transfer to the first excited state of ^{33}S and for the proton-pickup reaction seem to reproduce the gross features of the observed cross sections but not the details.

B. Reactions induced on ^{28}Si

The observed angular distributions for the reaction $^{28}Si(^{13}C, ^{12}C)^{29}Si$ leading to the ground state and first excited state of ^{29}Si are shown in Fig. 7 along with two different EFR DWBA calculations for each state. The solid line corresponds to the EFR DWBA calculations with the distorted wave in the entrance channel calculated from optical-model parameters for the elastic scattering of 36 MeV ^{13}C incident on ^{28}Si and the optical-model parameters for the elastic scattering of 40 MeV ^{12}C incident on ^{28}Si used to calculate the distorted wave in the exit channel. The dashed line corresponds to the EFR DWBA calculations performed with the optical-model parameters for ^{13}C incident on ^{28}Si being used in both channels.

The scattering of ^{12}C from ^{28}Si was chosen to represent the exit-channel distorted wave in the same spirit in which the proton distorted wave in a (d, p) reaction is described by elastic scattering of protons from the target nucleus. The elastic scattering $^{12}C + ^{28}Si$ was measured at 40.16 MeV to give the same center-of-mass energy as the $^{12}C + ^{29}Si$ system.

In Table II, "same" and "different" for the derived spectroscopic factors for these two reac-

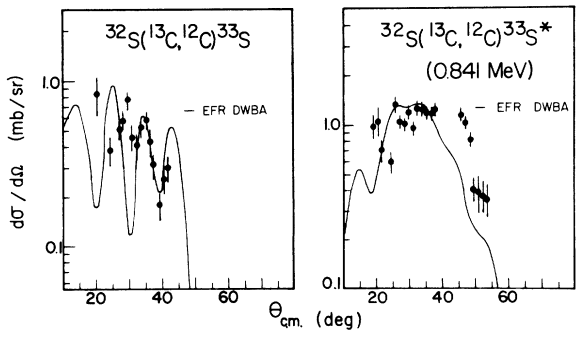

FIG. 5. Cross sections for the neutron-transfer reaction $^{32}S(^{13}C, ^{12}C)^{33}S$ leading to the ground state and the first excited state of ^{33}S, respectively. The solid line shows angular distributions predicted by EFR DWBA calculations.

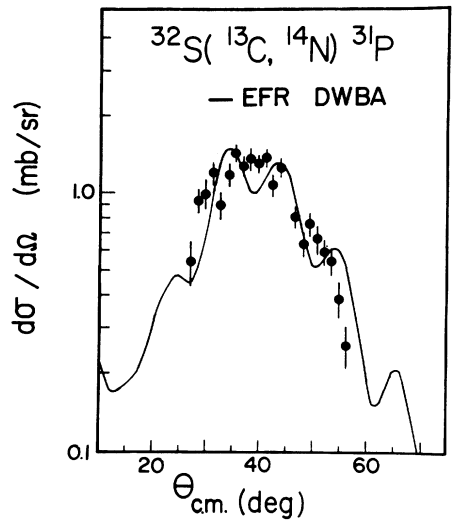

FIG. 6. Cross sections for the proton-pickup reaction $^{32}S(^{13}C, ^{14}N)^{31}P$ leading to the ground state of ^{31}P. The solid line shows the angular distribution predicted by EFR DWBA.

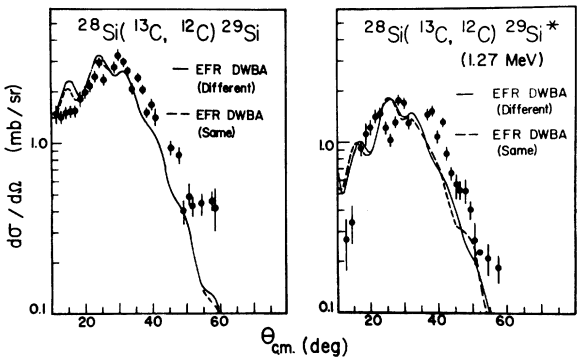

FIG. 7. Cross sections for the neutron-transfer reaction $^{28}Si(^{13}C, ^{12}C)^{29}Si$ leading to the ground state and the first excited state of ^{29}Si, respectively. The dashed curve shows EFR DWBA calculations in which the optical-model parameters in the exit channel were taken to be the same as those in the entrance channel. The solid line represents EFR DWBA calculations in which the optical-model parameters for the exit channel were chosen to fit the elastic scattering of 40.16 MeV ^{12}C from ^{28}Si. This corresponds to the energy of the exit channel consisting of ^{12}C and ^{29}Si in the above reaction leading to the ground state.

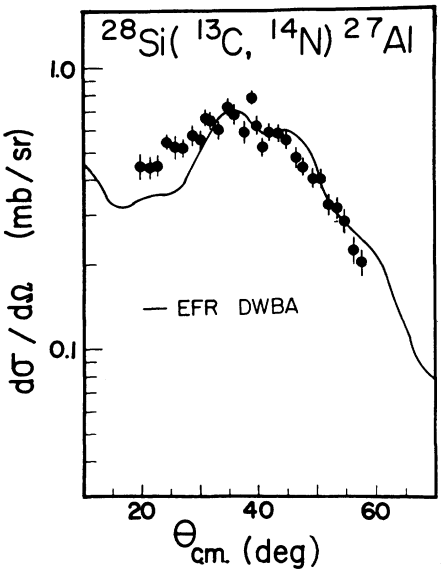

FIG. 8. Cross sections for the proton-pickup reaction ^{28}Si(^{13}C, ^{14}N)^{27}Al leading to the ground state of ^{27}Al. The solid line represents the angular distribution predicted by the EFR DWBA calculation.

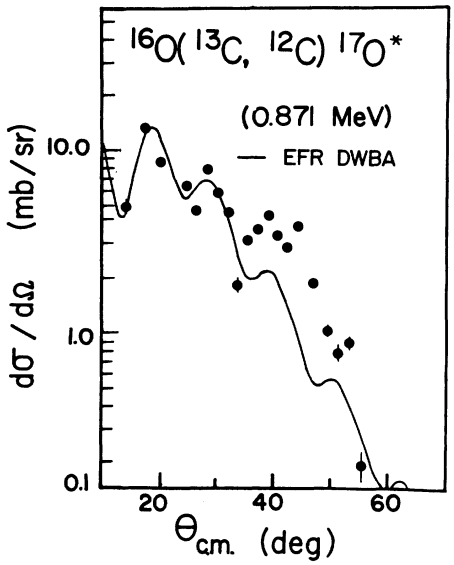

FIG. 9. Cross section for the neutron-transfer reaction ^{16}O(^{13}C, ^{12}C)^{17}O leading to the first excited state of ^{17}O. The solid line shows the angular distribution predicted by the EFR DWBA calculation.

tions refer to the choice of optical potentials in the entrance and exit channels as explained above.

For both the ground state and the first excited state, both EFR DWBA calculations, "same" and "different," predict similar angular distributions. Thus the calculations are not very sensitive to the optical-model parameters used in the exit channel. The calculations for the ground state predict the overall features of the observed data but fail to reproduce the details of the angular distribution. The agreement between the predicted and observed cross sections for the first excited state is poorer than that for the ground state. The oscillations in the data seem to be out of phase from the predicted oscillations.

Figure 8 shows the observed angular distribution for the proton-pickup reaction ^{28}Si(^{13}C, ^{14}N)^{27}Al. The EFR DWBA calculation shown as a solid line in this figure describes the data well except at forward angles where the predicted cross section is too low.

C. ^{13}C induced reactions on ^{16}O

Experimental cross sections for the reaction ^{16}O(^{13}C, ^{12}C)^{17}O* leading to the first excited state of ^{17}O are shown in Fig. 9 where the solid line corresponds to an EFR DWBA calculation. The overall shape of the EFR DWBA calculation reproduces the gross features of the data but it fails to predict the cross section from 30° to 60° where the prediction is too low.

D. ^{13}C induced reactions on ^{12}C

The measured cross sections for the α-transfer reaction ^{12}C(^{13}C, ^{9}Be)^{16}O are shown in Fig. 10. The angular distribution displays strong oscillations that are superimposed upon a gradual decrease of

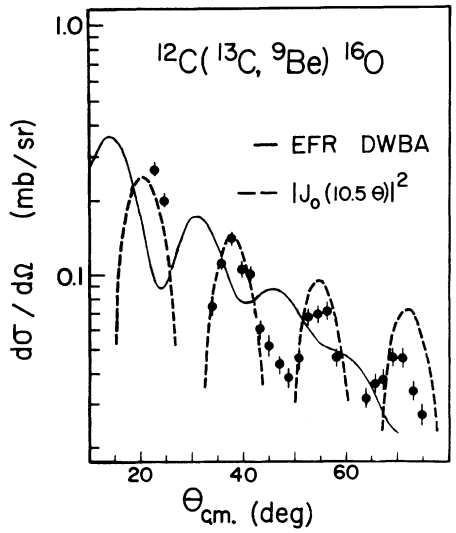

FIG. 10. Cross sections for the α-transfer reaction ^{12}C(^{13}C, ^{9}Be)^{16}O leading to the ground states of ^{16}O and ^{9}Be. The solid line represents EFR DWBA calculation based upon a cluster-model form factor. The dashed line stands for $[J_0(10.5\theta)]^2$ multiplied by a suitable constant to give a visual fit to the data. Here $[J_0(10.5\theta)]^2$ is used as a convenient approximation for $[P_{10}(\cos\theta)]^2$.

the cross section with angle. The solid line is the prediction of the EFR DWBA based on the assumption that the four nucleons are transferred as an α particle. In this model, the form factor for the α particle is determined by specifying its orbital angular momentum L and the number of nodes N in the radial part of the wave function. The quantum numbers assumed to describe the cluster bound to ^{12}C to produce ^{16}O are $N=2$ (excluding the one at the origin) and $L=0$. Similarly, the quantum numbers describing the α cluster around ^{9}Be are $N=1$ and $L=2$. The parameters of the Saxon-Woods potential were taken to be $r_0=1.0$ fm and $a=0.65$ fm. The radius parameter of the well R, was taken to be $r_0(A_1^{1/3}+A_2^{1/3})$. The well depths of the single-particle potentials used to bind the α particles to the respective cores were 47.93 MeV for $^{12}C+\alpha$ system and 56.49 MeV for $^{9}Be+\alpha$ system. The calculated cross sections bear little resemblance to the data. We performed some calculations with other values for the parameter r_0 (20% changes). However, the results did not agree better with experimental cross sections.

Following Ref. 23 we computed $[J_0((l_0+\frac{1}{2})\theta)]^2$, which is a good approximation to $[P_{l_0}(\cos\theta)]^2$, where l_0 is given by the expression

$$l_0+\tfrac{1}{2}=\eta\cot(\tfrac{1}{2}\theta_0) \tag{6}$$

and θ_0 is defined by the relation

$$\sigma_{el}(\theta_0)/\sigma_R(\theta_0)=\tfrac{1}{4}\,, \tag{7}$$

η stands for the Sommerfeld parameter, and θ_0 is the angle often referred to as the "quarter-angle." For our case $l_0=10$, the corresponding prediction for the angular distribution is shown as a dotted line in Fig. 10. The fit is quite good. It remains, however, to understand why ^{9}Be is ejected in almost an eigenstate of orbital angular momentum.

V. CONCLUSION

Elastic scattering data obtained in this experiment could be fitted very well with reasonable values of optical-model parameters. There are some discrepancies between theory and experiment for the elastic scattering from ^{12}C and ^{16}O. These might be due to elastic-transfer amplitude or inelastic scattering effects. Finally, these discrepancies might reflect the difficulty of describing elastic scattering from light nuclei in terms of optical potentials, a problem well known from work with light ions. Calculations of the cross section for the reaction $^{28}Si(^{13}C,^{12}C)^{29}Si$ showed that for small changes of optical-model parameters (10% change in real well depth) about the values found in this work, the calculated reaction cross sections remained essentially the same (within a few percent) if the changed optical-model parameters also fitted the elastic scattering. The EFR DWBA calculations compare reasonably well with the data but failed to reproduce the detailed shape of the angular distributions. It is possible that very different optical-model parameters exist that lead to an equally good fit to elastic scattering data and in conjunction with the EFR DWBA code provide better fit to the reaction data.

Spectroscopic factors obtained for the ground state and first excited state of ^{33}S from the neutron-transfer reactions are about 1.5 times the values obtained from (d,p) studies. The reaction $^{16}O(^{13}C,^{12}C)^{17}O^*$ (0.871 MeV) yielded a spectroscopic factor about 0.5 times the value obtained from (d,p) reaction studies. We do not have a specific explanation for these discrepancies at this time. Measured angular distributions for the α-transfer reaction $^{12}C(^{13}C,^{9}Be)^{16}O$ bear little resemblance to the EFR DWBA based on the cluster-model form factor. The measured angular distribution is, however, well fitted by the function $|P_{10}(\cos\theta)|^2$. Thus ^{9}Be is produced in almost an eigenstate of orbital angular momentum with $l=10$ which is the orbital angular momentum for the trajectory of ^{13}C for a grazing collision as determined by semiclassical considerations.

After this manuscript was completed, a paper by A. J. Baltz, P. D. Bond, J. D. Garrett, and S. Kahana[24] appeared in print. The improved optical-model potential proposed by these authors might well be important for our analysis as indicated by a sample calculation, the results of which were communicated to us by Mr. R. Landon Ray.

We wish to acknowledge stimulating discussions with W. R. Coker. We also wish to thank Mr. R. Landon Ray for help in the use of the EFR DWBA code.

---

†Work supported in part by the U.S. Energy Research and Development Administration.

*Present address: Lawrence Berkeley Laboratory, Nuclear Chemistry Division, Berkeley, California.

[1]H. Körner, G. Morrison, L. Greenwood, and R. Siemssen, Phys. Rev. C 7, 107 (1973).

[2]M. Schneider, C. Chasman, E. Auerbach, A. Baltz, and S. Kahana, Phys. Rev. Lett. 31, 320 (1973).

[3]P. D. Bond, J. D. Garrett, O. Hansen, S. Kahana, M. LeVine, and A. Schwarzschild, Phys. Lett. 47B, 231 (1973).

[4]P. R. Christensen, V. Manko, F. Becchetti, and R. Nickles, Nucl. Phys. A207, 33 (1973).

[5]W. von Oertzen, in *Nuclear Spectroscopy and Reactions,*

edited by J. Cerny (Academic, New York, 1974), Vol. IV, Pt. B, p. 280 and references therein.
[6]R. A. Broglia and A. Winther, Phys. Rep. 4C, 155 (1972).
[7]V. M. Strutinsky, Zh. Eksp. Teor. Fiz. 46, 2078 (1964) [Sov. Phys. JETP 19, 1401 (1964)].
[8]V. M. Strutinsky, Phys. Lett. 44B, 245 (1973).
[9]H. L. Harney P. Braun-Munzinger, and C. K. Gelbke, Z. Phys. 269, 339 (1974).
[10]T. Tamura and K. S. Low, Comp. Phys. Comm. 8, 349 (1974).
[11]R. M. De Vries, Phys. Rev. C 8, 951 (1973).
[12]A. Gobbi, in *Proceedings of the International Conference on Reactions between Complex Nuclei*, edited by R. L. Robinson, F. K. McGowan, J. B. Ball, and J. H. Hamilton (North-Holland, Amsterdam, 1974), Vol. 2, p. 211.
[13]L. Chua, A. Gobbi, R. Weiland, M. W. Sachs, D. Shapira, R. G. Stockstad, and D. A. Bromley, in *Proceedings of the International Conference on Nuclear Physics*, edited by J. de Boer and H. J. Mang (North-Holland, Amsterdam, 1973), Vol. 1, p. 345.
[14]P. T. Debevec, H. J. Körner, and J. P. Schiffer, Phys. Rev. Lett. 31, 171 (1973).
[15]H. P. Seiler, R. Kulessa, P. M. Cockburn, and P. Marmier, Nucl. Phys. A241, 151 (1975); A241, 159 (1975).
[16]R. Middleton (private communication).
[17]L. C. Northcliffe and R. F. Schilling, Nucl. Data A7, 233 (1970).
[18]W. R. Coker (private communication).
[19]G. Igo, Phys. Rev. 115, 1665 (1959).
[20]J. B. Ball, O. Hansen, J. S. Larsen, D. Sinclair, and F. Videback, Nucl. Phys. A244, 341 (1975).
[21]J. Schiffer, G. Morrison, R. Siemssen, and B. Zeidman, Phys. Rev. 164, 1274 (1967), and references therein.
[22]S. Cohen and D. Kurath, Nucl. Phys. A101, 1 (1967).
[23]P. Braun-Munzinger, W. Bohne, C. K. Gelbke, W. Grochulski, H. L. Harney, and H. Oeschler, Phys. Rev. Lett. 31, 1423 (1973).
[24]A. J. Baltz, P. D. Bond, J. D. Garrett, and S. Kahana, Phys. Rev. C 12, 136 (1975).
[25]M. C. Mermaz, C. A. Whitten, Jr., J. W. Champlin, A. J. Howard, and D. A. Bromley, Phys. Rev. C 4, 1778 (1971).
[26]M. D. Cooper, W. F. Hornyak, and P. G. Roos, Nucl. Phys. A218, 249 (1974).
[27]J. L. Alty, L. L. Green, R. Huby, G. D. Jones, J. R. Mines, and J. F. Sharpey-Schafer, Nucl. Phys. A97, 541 (1967).
[28]I. M. Naqib and L. L. Green, Nucl. Phys. A112, 76 (1968).
[29]G. Th. Kaschl, G. Mairle, U. Schmidt-Rohr, G. J. Wagner, and P. Turek, Nucl. Phys. A136, 286 (1969).
[30]M. Arditi, L. Bimbot, H. Doubre, N. Frascaria, J. P. Garron, M. Riou, and D. Royer, Nucl. Phys. A165, 129 (1971).